XLI CILAMCE
XLI Ibero-Latin American Congress on Computational Methods in Engineering
16-19 November, 2020 FOZ DO IGUAÇU PARANÁ - BRAZIL

Nonlinear analysis of viscoelastic rectangular plates subjected to harmonic in-plane load compression

Phablo V. I. Dias[1], Zenón J. G. N. del Prado[1], Renata M. Soares[1]

[1]*School of Civil and Environmental Engineering, Federal University of Goiás*
Avenida Universitária, 1488, Setor Leste Universitário, 74605-200, Goiânia, GO, Brazil
phablo@discente.ufg.br, zenon@ufg.br, renatasoares@ufg.br

Abstract. In this work, based on Kelvin-Voigt mechanical model, the viscoelastic damping on the dynamic instability of axially loaded rectangular plates is studied. A thin stainless-steel rectangular plate with linear rotational springs at the edges is considered. The non-linear Von-Kármán relations are used to describe the deformation relations of plates and the system of non-linear dynamic equilibrium equations is found through the Hamilton principle by application of the Rayleigh-Ritz method, which are in turn, solved by the fourth-order Runge-Kutta method. The bifurcation diagrams, the phase portraits and the Poincaré maps are obtained for the principal and secondary instability regions. For lower values of axial loading, the non-trivial solutions analyzed in the secondary region of dynamic instability are characterized by two periodic responses of period 1T, at the principal instability region, a periodic solution of period 2T is observed. When the plate is analyzed with higher levels of axial loading, this response may have periods of high order, and quasi-periodic and chaotic responses are also found.

Keywords: Viscoelastic Plates, Kelvin-Voigt Model, Bifurcation Diagrams.

1 Introduction

Plates are structural systems defined with bi-dimensional coordinates with one of its dimensions much smaller than others and, depending in the imposed loads, they can display complex nonlinear vibrations. Some plates are composed with materials such as rubber or biomaterials, and display gradative deformations in time when subjected to constant stress, which means a dissipative viscoelastic behavior.

A viscoelastic behavior is characterized by time depending constitutive equations and is composed by both elastic and damped terms. The viscoelastic analysis can be considered in several engineering areas such as damping in structures, where viscoelastic models can be used to describe damping. Amabili [1] and Flügge [2], indicate that one of the ways to perform viscoelastic analysis is considering a mechanical model such as: Kelvin-Voigt, Zener or Boltzmann.

Amabili [3] applied the Kelvin-Voigt model to study the non-linear vibrations of rectangular plates and compared viscoelastic damping with viscous damping observing that, the frequency response is different for different levels of damping. Balasubramanian et al [4] studied the influence of viscoelastic damping in rubber plates considering the Kelvin-Voigt material model and comparing numerical and experimental results. It was observed that the Kelvin-Voigt has some limitations for large amplitude oscillations were it is necessary to increase the viscoelastic parameter to find convergence between numerical and experimental results.

Amabili [5] presented a model applying the Zener to consider nonlinear damping. In this model it is possible to describe the nonlinear dynamic behavior of plates for different non-linearity levels considering only two damping coefficients. Other studies considering viscoelastic models can be found in Xia and Lukasiewicz [6, 7], Sun and Zhang [8] and Del Prado, Soares and Dias [9].

In this work the Kelvin-Voigt viscoelastic model is applied to study the nonlinear vibrations of clamped steel rectangular plates subjected to axial harmonic loads and to describe the clamped boundary conditions, rotational spring are considered. The Rayleigh-Ritz method together with the modified Hamilton principle are used to obtain a set of nonlinear dynamic equilibrium equations which are solved by the Runge-Kutta method. The bifurcation diagrams are obtained for the principal and secondary instability regions. A detailed study of response periodicity is performed to evaluated the effect of damping on the nonlinear response.

2 Mathematical Formulation

Consider a rectangular perfect clamped viscoelastic plate with coordinates (*x; y; z*) and displacement fields *u*, *v* and *w*, respectively with origin (*O*) at the corner of the plate. The plate has dimension *a*, *b*, thickness *h*, density ρ, Young modulus *E* and is subjected to and axial harmonic force with amplitude $N_{x,1}$ and frequency Ω as shown in Fig. 1 (Del Prado, Soares and Dias [9]).

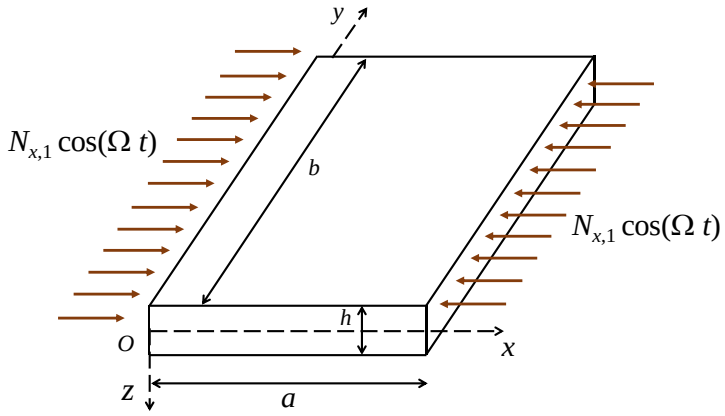

Figure 1. Viscoelastic plate under harmonic axial load

The non-linear strain-displacement relations of the mean surface and the changes of curvature can be described using the Von-Kármán theory (Amabili [10]) as given by:

$$\begin{aligned}
&\varepsilon_x = \varepsilon_{x,0} + zk_x, \quad \varepsilon_y = \varepsilon_{y,0} + zk_y, \quad \gamma_{xy} = \gamma_{xy,0} + zk_{xy} \\
&\varepsilon_{x,0} = \frac{\partial u}{\partial x} + \frac{1}{2}\left(\frac{\partial w}{\partial x}\right)^2, \quad \varepsilon_{y,0} = \frac{\partial v}{\partial y} + \frac{1}{2}\left(\frac{\partial w}{\partial y}\right)^2, \quad \gamma_{xy,0} = \frac{\partial u}{\partial x} + \frac{\partial v}{\partial y} + \frac{\partial w}{\partial x}\frac{\partial w}{\partial y} \\
&k_x = -\frac{\partial^2 w}{\partial x^2}, \quad k_y = -\frac{\partial^2 w}{\partial y^2}, \quad k_{xy} = -2\frac{\partial^2 w}{\partial x \partial y}
\end{aligned} \tag{1}$$

where ε_x, ε_y e γ_{xy} are the strain componentes at any point of the plate, and are related to the mean surfasse by ε_{x0}, ε_{y0} e $\gamma_{xy,0}$ and changes of curvature and torsion at the mean surface are k_x, k_y e k_{xy}.

The Kelvin-Voigt mechanical model is considered to describe the viscoelastic behavior of the plate, and the constitutive equation is given by:

$$\begin{aligned}
\sigma_x &= \frac{E}{1-\nu^2}\left(\varepsilon_x + \nu\,\varepsilon_y\right) + \eta\frac{E}{1-\nu^2}\left(\frac{\partial \varepsilon_x}{\partial t} + \nu\frac{\partial \varepsilon_y}{\partial t}\right) \\
\sigma_y &= \frac{E}{1-\nu^2}\left(\varepsilon_y + \nu\,\varepsilon_x\right) + \eta\frac{E}{1-\nu^2}\left(\frac{\partial \varepsilon_y}{\partial t} + \nu\frac{\partial \varepsilon_x}{\partial t}\right) \\
\tau_{xy} &= \frac{E}{2(1-\nu)}\left(\gamma_{xy}\right) + \eta\frac{E}{2(1-\nu)}\left(\frac{\partial \gamma_{xy}}{\partial t}\right)
\end{aligned} \tag{2}$$

where *E* is the Young modulus and η is the viscoelasticity coefficient given in seconds (*s*).

The potential energy of the plate is:

$$U_P = \frac{1}{2}\int_{\frac{-h}{2}}^{\frac{h}{2}}\int_0^a\int_0^b (\sigma_x\varepsilon_x + \sigma_y\varepsilon_y + \tau_{xy}\gamma_{xy})\,dxdydz \tag{3}$$

Substituting eq (1) and eq (2) in eq (3), the energy functional of the viscoelastic plate can be obtained and it can be described by the sum of the elastic (U_E) and viscoelastic (U_V) terms, as given by:

$$
\begin{aligned}
U_E &= \frac{Eh}{2(1-\nu^2)}\int_0^a\int_0^b\left(\varepsilon_{x,0}{}^2+\varepsilon_{y,0}{}^2+2\nu\varepsilon_{x,0}\varepsilon_{y,0}+\frac{1-\nu}{2}\gamma_{xy,0}{}^2\right)dxdy \\
&+\frac{Eh^3}{2(12(1-\nu^2))}\int_0^a\int_0^b\left(k_x{}^2+k_y{}^2+2\nu k_x k_y+\frac{1-\nu}{2}k_{xy}{}^2\right)dxdy \\
U_V &= \eta\frac{Eh}{(1-\nu^2)}\int_0^a\int_0^b\left(\varepsilon_{x,0}\dot{\varepsilon}_{x,0}+\varepsilon_{y,0}\dot{\varepsilon}_{y,0}+\nu\varepsilon_{x,0}\dot{\varepsilon}_{y,0}+\nu\varepsilon_{y,0}\dot{\varepsilon}_{x,0}+\frac{1-\nu}{2}\gamma_{xy,0}\dot{\gamma}_{xy,0}\right)dxdy \\
&+\eta\frac{Eh^3}{12(1-\nu^2)}\int_0^a\int_0^b\left(k_x\dot{k}_x+k_y\dot{k}_y+\nu k_x\dot{k}_y+\nu k_y\dot{k}_x+\frac{1-\nu}{2}k_{xy}\dot{k}_{xy}\right)dxdy
\end{aligned}
\tag{4}
$$

Rotational springs with stiffness k_r are placed in all boundaries of the plate, then, its potential energy (U_M) is:

$$
U_M = \frac{1}{2}\int_0^b k_r\left(\left(\left(\frac{\partial w}{\partial x}\right)_{x=0}\right)^2+\left(\left(\frac{\partial w}{\partial x}\right)_{x=a}\right)^2\right)dy+\frac{1}{2}\int_0^a k_r\left(\left(\left(\frac{\partial w}{\partial y}\right)_{x=0}\right)^2+\left(\left(\frac{\partial w}{\partial y}\right)_{x=b}\right)^2\right)dx \tag{5}
$$

Finally, the total potential energy of the plate results in:

$$
U = U_P + U_M \tag{6}
$$

If $k_r = 0$ we have a simply-supported plate and for a very high value of k_r we have a fully clamped plate. When comparing numerical and experimental results, it is necessary to make a convergence analysis to find the correct value of k_r, this is done when the experimental and numerical natural frequency are compared. The in-plane boundary conditions with axial moving supports, is considered to represent the simply-supported plate with moving boundaries (Amabili [10]). Then, to satisfy all boundary conditions, the following *u*, *v* and *w* fields displacements are adopted:

$$
\begin{aligned}
u(x,y,t) &= \sum_{m=1}^{M}\sum_{n=1}^{N}u_{m,n}(t)\cos\left(\frac{m\pi x}{a}\right)\sin\left(\frac{n\pi y}{b}\right) \\
v(x,y,t) &= \sum_{m=1}^{M}\sum_{n=1}^{N}v_{m,n}(t)\sin\left(\frac{m\pi x}{a}\right)\cos\left(\frac{n\pi y}{b}\right) \\
w(x,y,t) &= \sum_{m=1}^{M}\sum_{n=1}^{N}w_{m,n}(t)\sin\left(\frac{m\pi x}{a}\right)\sin\left(\frac{n\pi y}{b}\right)
\end{aligned}
\tag{7}
$$

where *m* e *n* are respectively the half-wave numbers in *x* and *y* directions; *M* and *N* are the number of terms used in each field displacement and $u_{m,n}(t)$, $v_{m,n}(t)$ e $w_{m,n}(t)$ are the unknown amplitudes. The vector of generalized amplitudes is given by:

$$
\mathbf{q} = \left[u_{m,n}(t),\quad v_{m,n}(t),\quad w_{m,n}(t)\right]^T \tag{8}
$$

where the dimension of $\mathbf{q}$ is given by N_q, which is the total of degrees of freedom of all field displacement.

The work done by the axial external axial load along the boindaries $x = 0$, a is given by:

$$
W = N_{x,1}\cos(\Omega\, t)\int_0^a\int_0^b\left(\frac{1}{2}\left(\frac{\partial w}{\partial x}\right)^2\right)dy\,dx \tag{9}
$$

where $N_{x,1}$ is the load amplitude and Ω is the frequency of excitation.

The kinetic energy, disregarding rotational energy, is given by:

$$
T = \frac{1}{2}\rho h\int_0^b\int_0^a\left(\dot{u}^2+\dot{v}^2+\dot{w}^2\right)dxdy \tag{10}
$$

The Rayleigh-Ritz method together with the Hamilton principle are used to obtain the set of nonlinear dynamics equations as:

$$\frac{d}{dt}\left(\frac{\partial T}{\partial \dot{q}_j}\right)-\frac{\partial T}{\partial q_j}+\frac{\partial U}{\partial q_j}=\frac{\partial W}{\partial q_j}, \text{ for } 1 \leq j \leq N_q \tag{11}$$

$$\mathbf{M}\ddot{\mathbf{q}}+\left(\mathbf{G}+\mathbf{G}_2(q)+\mathbf{G}_3(q,q)\right)\dot{\mathbf{q}}+\left(\mathbf{K}+\mathbf{K}_2(q)+\mathbf{K}_3(q,q)\right)\mathbf{q}=\mathbf{F}\cos(\Omega t) \tag{12}$$

where $\mathbf{M}$ is the diagonal mass matrix of dimensions $N_q \times N_q$; $\mathbf{G}$, $\mathbf{G}_2(q)$ and $\mathbf{G}_3(q, q)$ are, the linear, quadratic and cubic viscoelastic damping matrix, respectively; $\mathbf{K}$, $\mathbf{K}_2(q)$ and $\mathbf{K}_3(q, q)$ are the linear quadratic and cubic stiffness matrix, respectively; $\mathbf{F}$ is the load vector and $\ddot{\mathbf{q}}$, $\dot{\mathbf{q}}$ and $\mathbf{q}$ are the acceleration, velocity and displacement vectors, respectively.

3 Numerical Results

In this analysis, a thin stainless-steel rectangular plate is considered. This plate was studied by Amabili [5] and has the following physical and geometrical properties: $a = 0.25$ *m*, $b = 0.24$ *m*, $h = 0.0005$ *m*, $E = 193$ *GPa*, $\rho = 8000$ *kg/m³* and $\nu = 0.29$. The rotational springs have the following equivalent stiffness $k_r = 100$ *N/rad* and the Kelvin-Voigt viscoelastic material has the dissipation parameter $\eta = 5\ 10^{-6}$ *s*, typical of light damped materials. The plate is subjected to an axial load at borders $x = 0, a$ as shown in Fig. 1. To model the plate, 22 degrees of freedom in the field displacements were considered as seen in Tab. 1. For this plate, the natural frequency of the plate $\omega_{1,1} = 391.41$ *rad/s* and the axial buckling load is found to be $N_{cr} = 3297.29$ *N/m*.

Table 1. Generalized coordinates utilized in the expansions of the displacements

Displacements	Generalized coordinates
u	$u_{1,1}$, $u_{1,3}$, $u_{3,1}$, $u_{3,3}$, $u_{1,5}$, $u_{5,1}$, $u_{3,5}$, $u_{5,3}$, $u_{5,5}$
v	$v_{1,1}$, $v_{1,3}$, $v_{3,1}$, $v_{3,3}$, $v_{1,5}$, $v_{5,1}$, $v_{3,5}$, $v_{5,3}$, $v_{5,5}$
w	$w_{1,1}$, $w_{1,3}$, $w_{3,1}$, $w_{3,3}$

Now, the escape mechanisms of the plate due to axial load will be discussed, all bifurcations diagrams were obtained using the brute force method (Del Prado [11]). Figure 2 displays the bifurcations diagrams due to incremental values of axial load in the main ($\Omega = 2.0\ \omega_{1,1}$) (Fig. 2c and 2d) and secondary ($\Omega = 1.0\ \omega_{1,1}$) (Fig. 2a and 2b) instability regions.

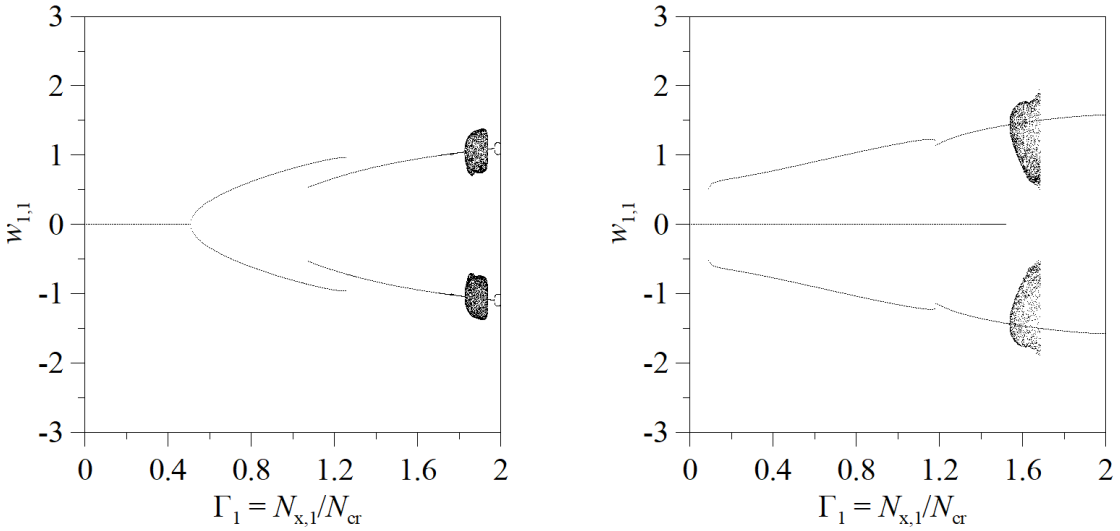

(a) $\Omega/\omega_{1,1} = 0{,}90$ (b) $\Omega/\omega_{1,1} = 1{,}05$

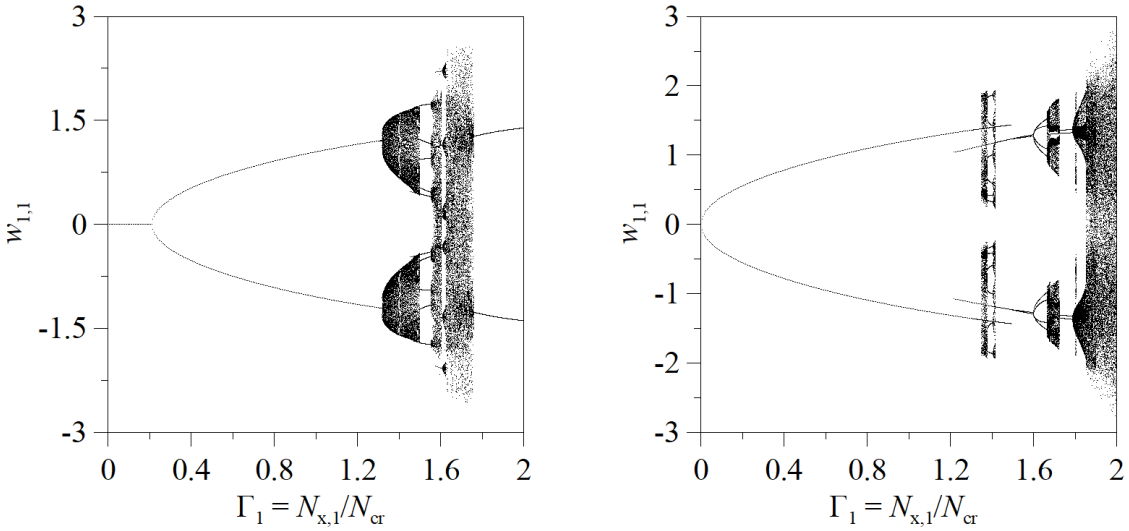

(c) $\Omega/\omega_{1,1}$ = 1,90 (d) $\Omega/\omega_{1,1}$ = 2,00

Figure 2. Bifurcation diagrams of stainless-steel plate

Figure 2a shows that for small values of the axial load, only trivial solutions of the plate are displayed. As the axial load is increased, at a critical value, the plate displays non-trivial solutions with super and sub-critical bifurcations. First, in Fig. 2a, the plate displays supercritical bifurcation, is the value of axial load is increased, the amplitude of vibrations are also increased with large amplitudes with a jump and a windows of quasi periodic solutions. In Fig. 2b, after trivial solutions, the plates shows a jump to large amplitude vibrations and also a window of quase periodic oscillations.

Now, for the main instability region in Fig. 2c, as the axial load is increased and at a critical point, the plate displays super-critical bifurcations with increasing values of amplitude vibrations. When the axial load continues to be increased, the plate shows windows with quasi periodic, chaotic and high periodic solutions. Finally, in Fig. 2d, the plate does not display trivial solutions but increasing periodic vibrations and, for large values of the axial load, there are windows with quasi periodic, chaotic and high periodic solutions. For example, at $\Gamma_1 = 1.40$ the plate shows quasi periodic oscillations and at $\Gamma_1 = 1.53$ the plate displays 10T periodic vibrations.

In Fig. 3, the phase portraits and Poincaré maps of some points of bifurcation diagrams of Fig. 2 are displayed. In the secondary region of dynamic instability, Fig. 3a shows the phase portraits and Poincaré maps corresponding to $\Omega/\omega_{1,1} = 0.90$ and $\Gamma_1 = 0.80$ of Fig. 2a, as can be observed, the plate shows two 1T (black and red dots) solutions. Now, Fig. 3b, displays mapping for $\Omega/\omega_{1,1} = 1.05$ and $\Gamma_1 = 0.80$ of Fig. 2b, at this load value it can be observed one trivial and two 1T periodic solutions. Quasi periodic oscillations can be observed at $\Omega/\omega_{1,1} = 1.05$ and $\Gamma_1 = 1.60$ from Fig. 2b at.

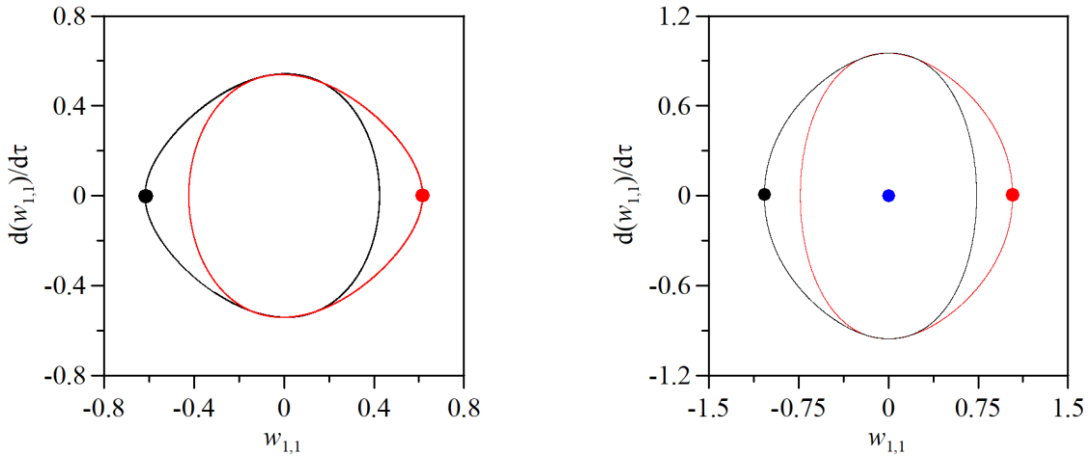

(a) Phase portraits and Poincaré maps at $\Omega/\omega_{1,1} = 0.90$ and $\Gamma_1 = 0.80$

(b) Phase portraits with Poincaré maps at $\Omega/\omega_{1,1} = 1.05$ and $\Gamma_1 = 0.80$

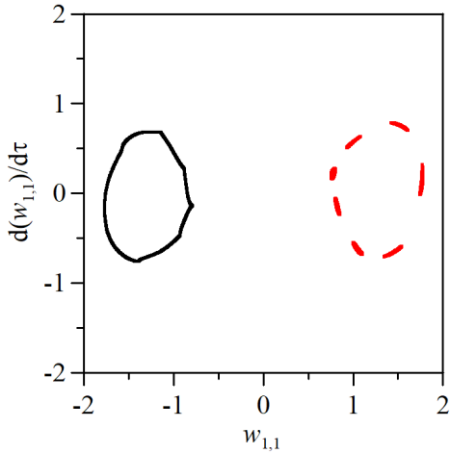

(c) Poincaré maps at $\Omega/\omega_{1,1}$= 1.05 and Γ_1 = 1.60

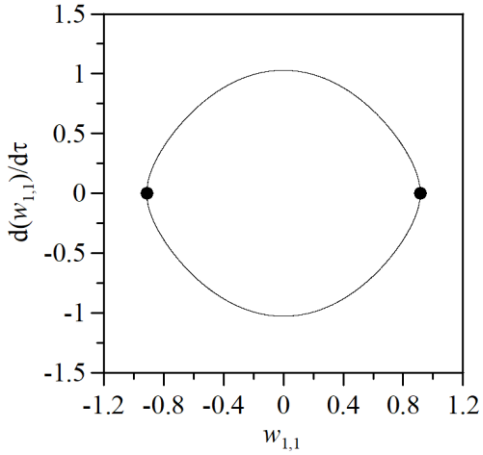

(d) Phase portraits with Poincaré maps at $\Omega/\omega_{1,1}$ = 1.90 and Γ_1 = 0.80

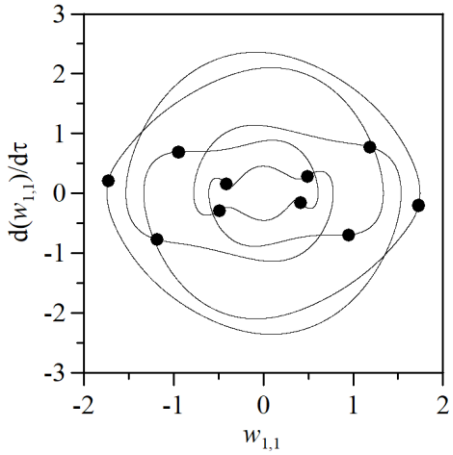

(e) Phase portraits with Poincaré maps at $\Omega/\omega_{1,1}$ = 1.90 and Γ_1 = 1.53

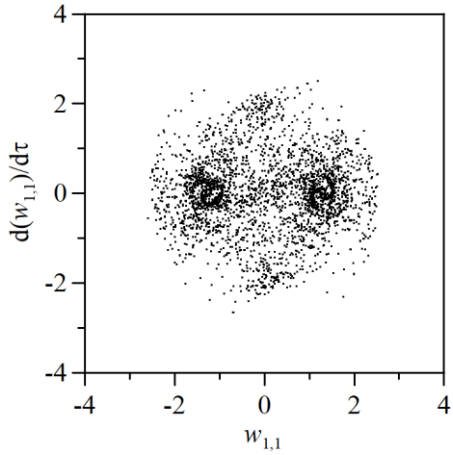

(f) Poincaré maps at $\Omega/\omega_{1,1}$ = 1.90 and Γ_1 = 1.70

Figure 3. Phase portraits and Poincaré maps of stainless-steel plate

Now at the main region of dynamic instability, Fig. 3d. display the mapping at $\Omega/\omega_{1,1}$ = 1.90 and Γ_1 = 0.80 from Fig. 2c, it is possible to observe one 2T stable periodic solution. At the other side, in Fig. 3e for $\Omega/\omega_{1,1}$ = 1.90 and Γ_1 = 1.53 from Fig. 2c, the plate shows 10T stable periodic solutions and finally, in Fig. 3f, at $\Omega/\omega_{1,1}$ = 1.90 and Γ_1 = 1.70 form Fig. 2c, the plate presents chaotic large amplitude vibrations.

4 Concluding Remarks

In a general way obtained results showed that for small values of the axial load (ex. Γ_1 = 0.8), the non-trivial solutions of the plate are characterized by two 1T periodic solutions in the secondary ($\Omega = 1.0\omega_{1,1}$) instability region. At the principal region of dynamic instability ($\Omega = 2.0\omega_{1,1}$) and for the same load level, the response of the plate is characterized by a 2T periodic solutions. For higher levels of axial load, it is possible to observe quasi periodic, chaotic and high period vibrations. Also, solutions found for the secondary region of instability, are more complex than solutions for the principal instability region.

Acknowledgements. This work was made possible by the support of the Coordination of Higher Level Personal Improvement – CAPES and Federal University of Goias computational laboratories.

Authorship statement. The authors hereby confirm that they are the sole liable persons responsible for the authorship of this work, and that all material that has been herein included as part of the present paper is either the property (and authorship) of the authors, or has the permission of the owners to be included here.

References

[1] M. Amabili. *Nonlinear Mechanics of Shells and Plates in Composite, Soft and Biological Materials*. Cambridge University Press, 2018. 582 p.
[2] W. Flügge, *Viscoelasticity.* Springer Science & Business Media, 2013. 204 p.
[3] M. Amabili, "Nonlinear vibrations of viscoelastic rectangular plates". *Journal Sound Vibrations.* v 362, p. 142–156, 2016.
[4] P. Balasubramanian, G. Ferrari, M. Amabili, Z. J. G. N. Del Prado, "Experimental and theoretical study on large amplitude vibrations of clamped rubber plates". *International Journal of Non-Linear Mechanics*, v 94, p. 36–45, 2017.
[5] M. Amabili, "Nonlinear damping in nonlinear vibrations of rectangular plates: Derivation from viscoelasticity and experimental validation". *Journal of the Mechanics and Physics of Solids*. v 118, p. 275–292, 2018.
[6] Z. Q. Xia, S. Lukasiewicz, "Non-linear, free, damped vibrations of sandwich plates". *Journal of Sound and Vibration***.** v 175, p. 219-232, 1994.
[7] Z. Q. Xia, S. Lukasiewicz, "Nonlinear damped vibrations of simply-supported rectangular sandwich plates". *Nonlinear Dynamics***.** v 8, p. 417–433, 1995.
[8] Y. X. Sun, S. Y. Zhang, "Chaotic dynamic analysis of viscoelastic plates". *International Journal of Mechanical Sciences.* v 43, p. 1195–1208, 2001.
[9] Z. J. G. N. del Prado, R. M. Soares, P. V. I. Dias, "Dynamic Instability of viscoelastic rectangular plates". In: *XL Ibero-Latin-American Congress on Computational Methods in Engineering (XL CILAMCE)*, Natal: UFRN, 2019, p. 1-10.
[10] M. Amabili. *Nonlinear Vibrations and Stability of Shells and Plates*. Cambridge University Press, 2008. 392 p.
[11] Z. J. G. N. Del Prado. *Acoplamento e interação modal na instabilidade dinâmica de cascas cilíndricas.* Tese (Doutorado em Engenharia Civil) – Departamento de Engenharia Civil, Pontifícia Universidade Católica do Rio de Janeiro, Rio de Janeiro, 2001.